J|A|C|S ARTICLES

Published on Web 10/06/2010

Origins of Hole Doping and Relevant Optoelectronic Properties of Wide Gap p-Type Semiconductor, LaCuOSe

Hidenori Hiramatsu,*,† Toshio Kamiya,‡ Tetsuya Tohei,§ Eiji Ikenaga,|| Teruyasu Mizoguchi,⊥ Yuichi Ikuhara,§,# Keisuke Kobayashi,∇ and Hideo Hosono†,‡

Frontier Research Center, S2-6F East, Mailbox S2-13, Tokyo Institute of Technology, 4259 Nagatsuta-cho, Midori-ku, Yokohama 226-8503, Japan, Materials and Structures Laboratory, Tokyo Institute of Technology, Yokohama 226-8503, Japan, Institute of Engineering Innovation, The University of Tokyo, Tokyo 113-8656, Japan, SPring-8, Japan Synchrotron Radiation Research Institute, 1-1-1 Kouto, Mikazuki-cho, Hyogo 679-5198, Japan, Institute of Industrial Science, The University of Tokyo, Tokyo 153-8505, Japan, Nanostructures Research Laboratory, Japan Fine Ceramics Center, Nagoya 456-8587, Japan, and SPring-8 Beamline Station, National Institute for Materials Science, 1-1-1 Kouto, Mikazuki-cho, Hyogo 679-5198, Japan

Received August 5, 2010; E-mail: h-hirama@lucid.msl.titech.ac.jp

Abstract: LaCuOSe is a wide band gap (~2.8 eV) semiconductor with unique optoelectronic properties, including room-temperature stable excitons, high hole mobility ~8 $cm^2/(Vs)$, and the capability of high-density hole doping (up to 1.7×10^{21} cm^{-3} using Mg). Moreover, its carrier transport and doping behaviors exhibit nonconventional results, e.g., the hole concentration increases with decreasing temperature and the high hole doping does not correlate with other properties such as optical absorption. Herein, secondary ion mass spectroscopy and photoemission spectroscopy reveal that aliovalent ion substitution of Mg at the La site is not the main source of hole doping and the Fermi level does not shift even in heavily doped LaCuOSe:Mg. As the hole concentration increases, the subgap optical absorption becomes more intense, but the increase in intensity does not correlate quantitatively. Transmission electron microscopy indicates that planar defects composed of Cu and Se deficiencies are easily created in LaCuOSe. These observations can be explained via the existence of a degenerate low-mobility layer and formation of complex Cu and Se vacancy defects with the assistance of generalized gradient approximation band calculations.

I. Introduction

In the past decade, wide gap oxide semiconductors have been intensively studied due to their unique optoelectronic functions. For example, Sn-doped In_2O_3 (ITO) exhibits high electrical conductivities, which are compatible with high transparency in the visible light region,[1] ZnO is expected for an emitting layer for blue near-ultraviolet light-emitting diodes (LEDs) due to its room-temperature stable excitons,[2,3] and a complex amorphous oxide, $InGaZnO_4$, has been applied to high-performance and transparent thin-film transistors (TFTs),[4] which are anticipated as a replacement for the amorphous silicon TFTs currently used in flat-panel displays. Among these applications, ITO has been used as a transparent anode (i.e., a hole-injection electrode), particularly in organic LEDs (OLEDs). Although ITO is an n-type conductor, it is used due to the absence of a transparent p-type anode material exhibiting an electrical conductivity and optical transparency comparable to those of ITO. We proposed that a wide gap p-type semiconductor would be a more suitable anode layer for OLEDs because the Fermi level (E_F) deepens for p-type semiconductors as the hole concentration increases, which should realize lower hole injection barriers as well as lower contact resistances. Because LaCuOSe is a wide gap (E_g ≈ 2.8 eV) p-type semiconductor[5] and Mg doping can achieve high-density hole doping up to 1.7×10^{21} cm^{-3},[6] it should be suitable as a wide gap p-type anode layer. Indeed, applying LaCuOSe:Mg epitaxial thin films as the anode layers in OLEDs has yielded a rather low hole injection barrier (~0.3 eV).[7] More recently, similar works have extended this strategy to include copper selenide grown at room temperature[8,9] and BaCuFSe[10,11]

† Frontier Research Center, S2-6F East, Mailbox S2-13, Tokyo Institute of Technology.
‡ Materials and Structures Laboratory, Tokyo Institute of Technology.
§ Institute of Engineering Innovation, The University of Tokyo.
|| Japan Synchrotron Radiation Research Institute.
⊥ Institute of Industrial Science, The University of Tokyo.
Japan Fine Ceramics Center.
∇ National Institute for Materials Science.

(1) Hamberg, I.; Granqvist, C. G. *J. Appl. Phys.* **1986**, *60*, R123.
(2) Ohta, H.; Kawamura, K.; Orita, M.; Hirano, M.; Sarukura, N.; Hosono, H. *Appl. Phys. Lett.* **2000**, *77*, 475.
(3) Nakahara, K.; Akasaka, S.; Yuji, H.; Tamura, K.; Fujii, T.; Nishimoto, Y.; Takamizu, D.; Sasaki, A.; Tanabe, T.; Takasu, H.; Amaike, H.; Onuma, T.; Chichibu, S. F.; Tsukazaki, A.; Ohtomo, A.; Kawasaki, M. *Appl. Phys. Lett.* **2010**, *97*, 013501.
(4) Nomura, K.; Ohta, H.; Takagi, A.; Kamiya, T.; Hirano, M.; Hosono, H. *Nature* **2004**, *432*, 488.
(5) Ueda, K.; Hosono, H. *J. Appl. Phys.* **2002**, *91*, 4768.
(6) Hiramatsu, H.; Ueda, K.; Ohta, H.; Hirano, M.; Kikuchi, M.; Yanagi, H.; Kamiya, T.; Hosono, H. *Appl. Phys. Lett.* **2007**, *91*, 012104.
(7) Yanagi, H.; Kikuchi, M.; Kim, K.-B.; Hiramatsu, H.; Kamiya, T.; Hirano, M.; Hosono, H. *Org. Electron.* **2008**, *9*, 890.
(8) Hiramatsu, H.; Koizumi, I.; Kim, K.-B.; Yanagi, H.; Kamiya, T.; Hirano, M.; Matsunami, N.; Hosono, H. *J. Appl. Phys.* **2008**, *104*, 113723.
(9) Yanagi, H.; Kim, K.-B.; Koizumi, I.; Kikuchi, M.; Hiramatsu, H.; Miyakawa, M.; Kamiya, T.; Hirano, M.; Hosono, H. *J. Phys. Chem. C* **2009**, *113*, 18379.

10.1021/ja107042r
© 2010 American Chemical Society

because their valence band maximum (VBM) structures are similar to that of LaCuOSe and are composed of antibonding states of Cu 3d and Se 4p admixed orbitals.[12−16]

Although we demonstrated that LaCuOSe can be applied to optoelectronic devices such as OLEDs[7] and excitonic blue LEDs,[17] the carrier transport/doping mechanism is not completely understood. Several contradicting electronic/optical properties and electronic structures have been observed. (I) Nominally undoped LaCuOSe exhibits a relatively high p-type conduction with hole concentrations up to 3×10^{19} cm^{-3},[18] and its temperature dependence of the Hall effect exhibits an abnormal behavior in which the hole concentration increases as the temperature decreases in the low-temperature region. (II) A Burstein−Moss (BM) shift[19,20] does not appear in the optical absorption (band filling effect) in LaCuOSe epitaxial thin films, even for highly doped LaCuOSe:Mg films (above 1×10^{21} cm^{-3}),[6] although a BM shift is common for other oxide conductors such as ITO[1] and amorphous $InGaZnO_4$.[21] (III) Doped LaCuOSe:Mg thin films exhibit a somewhat strong subgap optical absorption, which extends from the absorption edge in the range of 2.0−2.8 eV. (IV) Free hole absorption analyses provide a heavy effective mass value of $1.6m_e$ (m_e denotes the rest mass of electron), but the dispersion of the VBM band obtained by density functional theory (DFT) gives a much smaller value of $\sim 0.3m_e$.[6] (V) As discussed later, the Mg concentrations in heavily doped LaCuOSe:Mg thin films are too low to explain the free hole concentrations obtained by the Hall effect measurements. However, a high hole density has been attained only by Mg doping for thin films and not other aliovalent ion doping such as Sr and Ca. Therefore, a simple rigid-band model where mobile holes are generated by substituting Mg ions for La sites, which are then injected into the valence band (VB), cannot explain these contradicting results.

Herein, we first discuss the anomalous temperature dependence of the hole concentration using the coexistence of a low-mobility degenerated layer. Then the origin of hole doping is discussed based on the experimental results from near-infrared ultraviolet optical spectroscopy, hard X-ray photoemission spectroscopy (HX-PES), secondary ion mass spectroscopy (SIMS), and high-resolution transmission electron microscopy (HR-TEM). These results are inconsistent with substitution of aliovalent Mg ions at La sites as the source of hole doping but do suggest formation of complex Cu and Se defects in LaCuOSe. DFT calculations are used to elucidate stable defect structures, formation energies, and density of states (DOSs). These calculations are then employed to identify the origins of hole doping and the subgap optical absorption.

II. Experiments and Calculations

II.1. Fabrication and Characterization of Thin Films. Epitaxial thin films of nominally undoped (∼100 nm thick) and Mg-doped (∼100 and ∼40 nm thick) LaCuOSe were prepared on MgO (001) single-crystal substrates via reactive solid-phase epitaxy (R-SPE).[22] Amorphous LaCuOSe films were initially deposited on a sacrificial Cu layer (∼5 nm thick)/MgO (001) substrate. The obtained bilayer films were crystallized at 1000 °C in evacuated silica glass ampules. Solid-phase epitaxial growth converted the bilayer into epitaxial films of LaCuOSe with the assistance of the sacrificial Cu layer. Cu and amorphous LaCuOSe films were deposited by pulsed laser deposition (PLD) using polycrystalline disk targets of metal Cu, undoped LaCuOSe, and Mg-doped LaCuOSe with a chemical composition of $La_{0.8}Mg_{0.2}CuOSe$. Details of the film preparation procedure and crystalline qualities are reported elsewhere.[6,23−26]

The carrier transport properties (carrier concentration, n_{Hall}, and Hall mobility, μ_{Hall}) were examined by the Hall effect measurements in a temperature range of 30−300 K using the van der Pauw configuration under ac modulation of a magnetic field (model RESITEST 8300, Toyo Co.).

The optical transmission (T_{obs}) and normal reflectance (R_{obs}) spectra were measured at room temperature in the ultraviolet to near-infrared region with a conventional spectrophotometer (model U-4000, Hitachi Co.). The absorption coefficients (α) were evaluated from T_{obs} and R_{obs} using the relation $T_{obs}/(1 - R_{obs}) \approx \exp(-\alpha d)$, where d denotes the film thickness to correct the reflection loss.[27]

HX-PES was used to observe the VB electronic structures because a high-energy X-ray source is more sensitive to the deeper bulk region than conventional soft X-ray PES, i.e., HX-PES data is less affected by surface states and contamination.[28] The HX-PES measurements were performed at room temperature in beamline BL47XU (excitation energy = 7940 eV) at SPring-8. The kinetic energies obtained were calibrated by the E_F of a gold reference.

The chemical compositions of the films were determined by SIMS (IMS-6F made by CAMECA) using O_2^+ as the primary ion source. Polycrystalline disks of LaCuOSe and $La_{0.8}Mg_{0.2}CuOSe$, which were the PLD targets, were employed as standard samples to convert the secondary ion signals into atomic ratios.

Cross-sectional microscopic observations were performed by HR-TEM (model JEM-4010, JEOL Ltd.). Additionally, we also used a scanning transmission electron microscope (STEM) (model JEM-2100F, JEOL Ltd.) equipped with a spherical aberration corrector to achieve atomic resolution. High-angle annular dark-field (HAADF) observations were made using a ∼0.1 nm probe. During HAADF imaging, the probe convergence angle and HAADF collection angle were about 22 and 80−220 mrad, respectively. The TEM samples were prepared using a standard method, which employed mechanical grinding, dimpling, and Ar ion milling. To avoid damage due to electron irradiation during TEM observations, we carefully

(10) Zakutayev, A.; Tate, J.; Platt, H. A. S.; Keszler, D. A.; Barati, A.; Klein, A.; Jaegermann, W. *Appl. Phys. Lett.* **2010**, *96*, 162110.
(11) Zakutayev, A.; Tate, J.; Platt, H. A. S.; Keszler, D. A.; Hein, C.; Mayer, T.; Klein, A.; Jaegermann, W. *J. Appl. Phys.* **2010**, *107*, 103713.
(12) Ueda, K.; Hiramatsu, H.; Ohta, H.; Hirano, M.; Kamiya, T.; Hosono, H. *Phys. Rev. B* **2004**, *69*, 155305.
(13) Ueda, K.; Hosono, H.; Hamada, N. *J. Phys.: Condens. Matter* **2004**, *16*, 5179.
(14) Kamiya, T.; Ueda, K.; Hiramatsu, H.; Kamioka, H.; Ohta, H.; Hirano, M.; Hosono, H. *Thin Solid Films* **2005**, *486*, 98.
(15) Ueda, K.; Hosono, H.; Hamada, N. *J. Appl. Phys.* **2005**, *98*, 043506.
(16) Yanagi, H.; Tate, J.; Park, S.; Park, C.-H.; Keszler, D. A.; Hirano, M.; Hosono, H. *J. Appl. Phys.* **2006**, *100*, 083705.
(17) Hiramatsu, H.; Ueda, K.; Ohta, H.; Kamiya, T.; Hirano, M.; Hosono, H. *Appl. Phys. Lett.* **2005**, *87*, 211107.
(18) Hiramatsu, H.; Ueda, K.; Ohta, H.; Hirano, M.; Kamiya, T.; Hosono, H. *Appl. Phys. Lett.* **2003**, *82*, 1048.
(19) Burstein, E. *Phys. Rev.* **1954**, *93*, 632.
(20) Moss, T. S. *Proc. Phys. Soc. London, Sect. B* **1954**, *67*, 775.
(21) Kamiya, T.; Nomura, K.; Hosono, H. *J. Display Technol.* **2009**, *5*, 273.
(22) Ohta, H.; Nomura, K.; Orita, M.; Hirano, M.; Ueda, K.; Suzuki, T.; Ikuhara, Y.; Hosono, H. *Adv. Funct. Mater.* **2003**, *13*, 139.
(23) Hiramatsu, H.; Ueda, K.; Ohta, H.; Orita, M.; Hirano, M.; Hosono, H. *Appl. Phys. Lett.* **2002**, *81*, 598.
(24) Hiramatsu, H.; Ohta, H.; Suzuki, T.; Honjo, C.; Ikuhara, Y.; Ueda, K.; Kamiya, T.; Hirano, M.; Hosono, H. *Cryst. Growth Des.* **2004**, *4*, 301.
(25) Hiramatsu, H.; Ueda, K.; Takafuji, K.; Ohta, H.; Hirano, M.; Kamiya, T.; Hosono, H. *J. Mater. Res.* **2004**, *19*, 2137.
(26) Tohei, T.; Mizoguchi, T.; Hiramatsu, H.; Hosono, H.; Ikuhara, Y. *Mater. Sci. Eng., B* **2010**, *173*, 229.
(27) Hishikawa, Y.; Nakamura, N.; Tsuda, S.; Nakano, S.; Kishi, Y.; Kuwano, Y. *Jpn. J. Appl. Phys.* **1991**, *30*, 1008.
(28) Kobayashi, K. *Nucl. Instrum. Methods A* **2009**, *601*, 32.

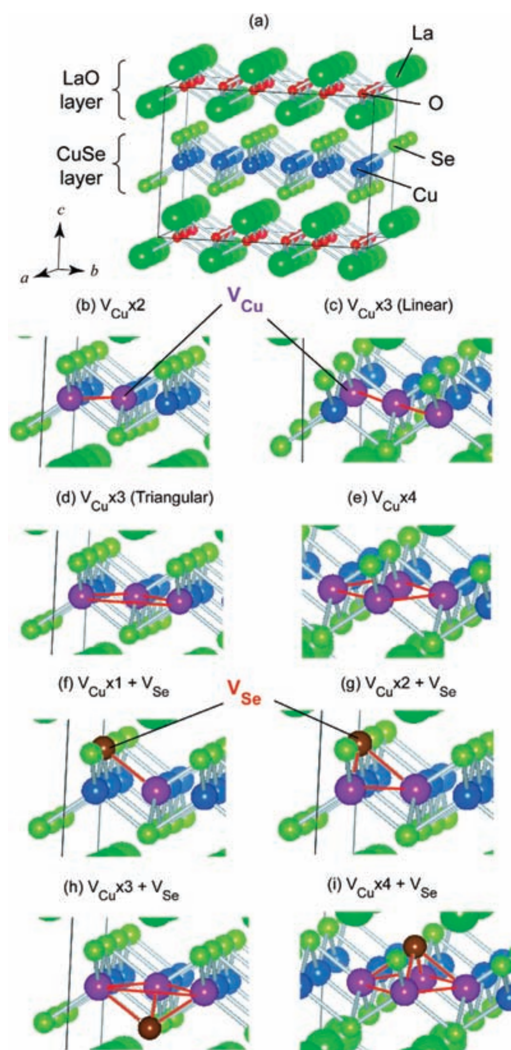

Figure 1. (a) 3 × 3 × 1 LaCuOSe supercell model is used as the base model for the defect calculations. (b−i) Defect models in the CuSe layer. (b) V_{Cu} × 2. (c) V_{Cu} × 3 (linear) (three V_{Cu} aligned linearly along the [110] direction). (d) V_{Cu} × 3 (triangle) (three V_{Cu} form a right triangle). (e) V_{Cu} × 4 (four squared Cu ions are removed). (f) Se and a bonding Cu ion are removed. (g) Se and two bonding Cu ions are removed. (h) Se and three bonding Cu ions are removed. (i) Se and four bonding Cu ions are removed.

verified the specimen condition and confirmed the reproducibility of the results.

II.2. Ab Initio Calculations. DFT periodic calculations were performed using the VASP code[29] with the projector augmented wave (PAW) method[30,31] and PBE96 generalized gradient approximation (GGA) functionals. To investigate the equilibrium structures and formation energies of dopants and defects in LaCuOSe, variable-cell relaxation calculations were performed for the following models: a stoichiometric cell model, doping models, point-defect containing models, and complex defect models. The base structure was a stoichiometric model possessing a $(LaCuOSe)_2$ conventional tetragonal unit cell.[32] The other models employed 3 × 3 × 1 supercells composed of $(LaCuOSe)_{18}$ as the base model (Figure 1a). The doping models were built by substituting an alkaline-earth ion (AE = Mg, Ca, and Sr) for a La ion (LaCuOSe: AE, $La_{17}AECu_{18}O_{18}Se_{18}$). The point-defect models included a monovacancy of a constituent ion ($La_{17}Cu_{18}O_{18}Se_{18}$ for V_{La}, $La_{18}Cu_{17}O_{18}Se_{18}$ for V_{Cu}, $La_{18}Cu_{18}O_{17}Se_{18}$ for V_O, and $La_{18}Cu_{18}O_{18}Se_{17}$ for V_{Se}) or an anion substitution defect ($La_{18}Cu_{18}O_{19}Se_{17}$ for O_{Se} and $La_{18}Cu_{18}O_{17}Se_{19}$ for Se_O). The complex defect models included clusters of V_{Cu} where the number of $V_{Cu}(x)$ varied from 1 to 4 (V_{Cu} × x) (Figure 1b−e) as well as clusters of V_{Cu} and V_{Se} where the number of V_{Cu} varied from 1 to 4 while that of V_{Se} was fixed at 1 (V_{Cu} × x + V_{Se}) (Figure 1f−i).

Quantum mechanically stable structures were obtained by optimizing the lattice parameters and atomic positions of the structure models so as to take the minimum total energies. To calculate formation energies of the defects (E_{Form}), the self-consistent field (SCF) total energies of the most stable elementary crystals were calculated for La, Cu, Se, Mg, Ca, and Sr after variable-cell relaxation. For O, the SCF total energy of the gas-phase O_2 was calculated for an O_2 molecule in a large cubic unit cell with a lattice parameter of 1.5 nm by a gamma point only periodic calculation after optimizing the O−O bond length. DOSs were calculated based on the relaxed structures. All DOSs were compared by normalizing the energy axis using the peak energies of the deep La 5s state at ca. −32 eV.

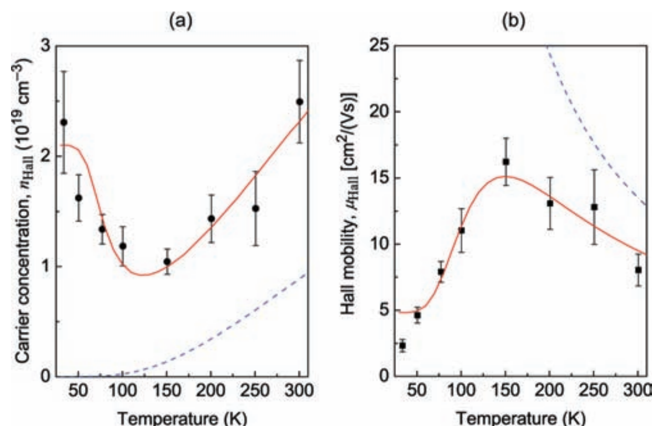

Figure 2. Temperature dependences of the carrier transport properties of nominally undoped LaCuOSe epitaxial films. (a) Carrier concentration (n_{Hall}) and (b) Hall mobility (μ_{Hall}). Error bars indicate standard errors of the Hall voltages. Red solid curves are the fitting results of the two-layer model, while blue dashed curves are those of the bulk region extracted from the two-layer model analysis.

III. Results

III.1. Anomalous Temperature Dependence of the Hole Concentration. Highly doped films with $n_{Hall} \geq 1 \times 10^{20}$ cm^{-3} exhibited degenerate conduction due to the high carrier concentrations (see Figure S1 in the Supporting Information),[6,18] i.e., both n_{Hall} and μ_{Hall} were nearly independent of temperature. In contrast, for nominally undoped epitaxial films with n_{Hall} = 2.5 × 10^{19} cm^{-3}, n_{Hall} increased as the temperature increased above 120 K (Figure 2). These observations are reasonably explained by thermal excitation of the holes from the acceptor level. However, these films exhibited an anomalous behavior in the lower temperature region where n_{Hall} increased as temperature decreased. Similar behaviors have been reported for other wide gap semiconductors such as GaN[33−35] and ZnO.[36−38]

(29) Kresse, G.; Furthmüller, J. *Phys. Rev. B* **1996**, *54*, 11169.
(30) Blöchl, P. E. *Phys. Rev. B* **1994**, *50*, 17953.
(31) Kresse, G.; Joubert, D. *Phys. Rev. B* **1999**, *59*, 1758.
(32) Zhu, W. J.; Huang, Y. Z.; Dong, C.; Zhao, Z. X. *Mater. Res. Bull.* **1994**, *29*, 143.
(33) Molnar, R. J.; Lei, T.; Moustakas, T. D. *Appl. Phys. Lett.* **1993**, *62*, 72.
(34) Look, D. C.; Molnar, R. J. *Appl. Phys. Lett.* **1997**, *70*, 3377.
(35) Xu, X. L.; Beling, C. D.; Fung, S.; Zhao, Y. W.; Sun, N. F.; Sun, T. N.; Zhang, Q. L.; Zhan, H. H.; Sun, B. Q.; Wang, J. N.; Ge, W. K.; Wong, P. C. *Appl. Phys. Lett.* **2000**, *76*, 152.

Look et al.[34] explained this anomaly by assuming the coexistence of a thin degenerated layer with a small mobility (a two layer model). Following their procedure, the observed μ_{Hall} and n_{Hall} can be expressed as

$$\mu_{Hall}(T) = \frac{\mu_{bulk}(T)^2 n_{bulk}(T) + \mu_2^2 n_2}{\mu_{bulk}(T) n_{bulk}(T) + \mu_2 n_2} \quad (1)$$

$$n_{Hall}(T) = \frac{[\mu_{bulk}(T) n_{bulk}(T) + \mu_2 n_2]^2}{\mu_{bulk}(T)^2 n_{bulk}(T) + \mu_2^2 n_2} \quad (2)$$

where $\mu_{bulk}(T)$ and μ_2 are the Hall mobilities and $n_{bulk}(T)$ and n_2 are hole concentrations. The subscripts bulk and 2 indicate the bulk layer and the thin degenerated layer, respectively. In this model, observed Hall voltages are governed by the bulk layer at high temperatures because $\mu_{bulk}(T)$ and $n_{bulk}(T)$ are larger than μ_2 and n_2 while the thin layer becomes dominant at low temperatures because $n_{bulk}(T)$ becomes very small, giving rise an anomalous behavior in carrier density. The temperature dependences of $\mu_{bulk}(T)$ and $n_{bulk}(T)$ were modeled based on the summation law of mobility and a single-acceptor level model, respectively

$$\frac{1}{\mu_{bulk}(T)} = \frac{1}{\mu_{01}T^{-1.5}} + \frac{1}{\mu_{02}T^{-1}} + \frac{1}{\mu_{03}T^{0}} + \frac{1}{\mu_{04}T^{1}} + \frac{1}{\mu_{05}T^{1.5}} \quad (3)$$

$$n_{bulk}(T) = \frac{N_A}{1 + \exp\left(\frac{E_A - E_F}{kT}\right)} \quad (4)$$

where μ_{0i} ($i = 1, ..., 5$) are constant prefactors, N_A is the acceptor concentration, E_A is the acceptor level, and k is the Boltzmann constant. μ_2 and n_2 were assumed to be temperature independent. The E_F was determined by the charge neutrality condition under a given temperature. The parameters μ_{0i}, N_A, E_A, μ_2, and n_2 were determined by the least-squares method so as to reproduce the observed temperature dependences of $\mu_{Hall}(T)$ and $n_{Hall}(T)$.

Figure 2 (red solid curves) shows the fitting results, indicating that the two-layer model well explains the observed temperature dependences of μ_{Hall} and n_{Hall} including the anomalous region < 120 K (symbols). The two-layer model yielded $N_A = 4.1 \times 10^{19}$ cm^{-3}, $E_A = 8$ meV, and μ_{bulk} at room temperature of 13 cm^2/(V s) (the blue dashed curves in Figure 2 depict the extracted $\mu_{bulk}(T)$ and $n_{bulk}(T)$). The mobility and sheet hole concentration of the thin degenerated layer were 4.8 cm^2/(V s) and 3.2×10^{14} cm^{-2}, respectively. Assuming a 1 nm thick layer, the sheet hole concentration corresponds to a volume concentration of 3.2×10^{21} cm^{-3}.

III.2. Rigid-Band Model or Impurity Band Model. Figure 3a shows the optical absorption spectra of LaCuOSe epitaxial films with different carrier concentrations of $n_{Hall} = 2.5 \times 10^{19}$ to 1.7×10^{21} cm^{-3} at 300 K. The $n_{Hall} = 2.5 \times 10^{19}$ film (nominally undoped sample) showed an optical absorption edge at ~2.8 eV. All films exhibited two peak shoulder structures just above the absorption edge (denoted A). These peaks originated from room-temperature stable excitons, and they were split by a spin−orbit (SO) interaction in the Se ions.[12,14] Nominally undoped LaCuOSe displayed a weak and broad absorption below the absorption edge (denoted B, subgap absorption), where the absorption became more intense as n_{Hall} increased. We performed optical model analyses using two Lorentz oscillators, which peaked at 2.75 and 2.5 eV, to obtain the fN_e values (f denotes the oscillator strength, and N_e is the concentration of electrons contributing to the absorption band).[6] The estimated values were $fN_e = 7 \times 10^{19}$ cm^{-3} for the $n_{Hall} = 2.5 \times 10^{19}$ cm^{-3} film, 6×10^{20} cm^{-3} for the 2.5×10^{20} cm^{-3} film, and 9×10^{20} cm^{-3} for the 1.7×10^{21} cm^{-3} film. The fN_e/n_{Hall} ratio drastically changed from 2.8 to 0.53, implying that the intensity of the subgap absorption band B is positively correlated to n_{Hall} but is controlled by more than n_{Hall}.

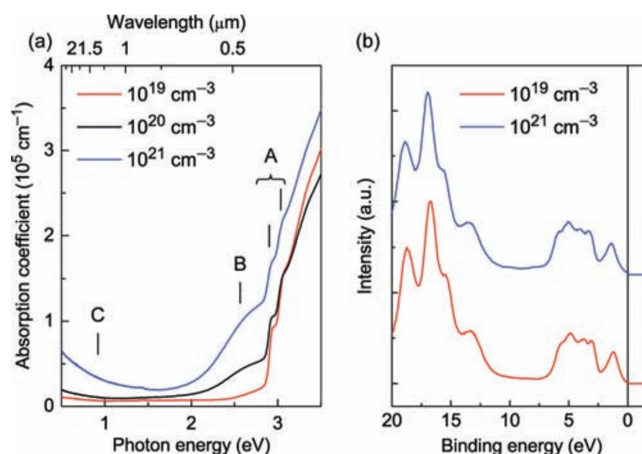

Figure 3. (a) Optical absorption spectra of LaCuOSe epitaxial films with carrier concentrations of $n_{Hall} = 2.5 \times 10^{19}$ to 1.7×10^{21} cm^{-3}: (black line) 100 nm thick nominally undoped LaCuOSe (n_{Hall} at 300 $K = 2.5 \times 10^{19}$ cm^{-3}), (red line) 100 nm thick LaCuOSe:Mg (2.2×10^{20} cm^{-3}), and (blue line) 40 nm thick LaCuOSe:Mg (1.7×10^{21} cm^{-3}). (b) HX-PES spectra of nominally undoped (2.5×10^{19} cm^{-3}, red line) and Mg-doped (1.7×10^{21} cm^{-3}, blue line) LaCuOSe films around the VB region. Energy is measured from the Fermi energies of the LaCuOSe films.

The absorption bands in the near-infrared region < 1.5 eV (denoted 'C') were assigned to free carrier absorption (FCA). FCA analysis of the $n_{Hall} = 1.7 \times 10^{21}$ cm^{-3} film using the Drude−Lorentz model clarified that the plasma frequency and momentum relaxation time were 1.8×10^{15} s^{-1} and 4.2×10^{-15} s, respectively. Using the carrier concentration obtained by Hall measurement ($n_{Hall} = 1.7 \times 10^{21}$ cm^{-3}), the estimated effective mass was $m_h^* \approx 1.6\, m_e$. On the other hand, the DFT calculations with a SO interaction gave a much smaller value of ~0.3 m_e at VBM.[6] The observed m_h^* may reflect the curvature of the VB band at a deep energy because the LaCuOSe:Mg film is heavily doped with a deep E_F and the VBM of LaCuOSe is largely distorted from the parabolic shape.[13,14] However, the experimental results implied that the locations of the absorption edge at ~2.8 eV and the exciton absorption peaks (A) did not shift even when n_{Hall} increased up to 1.7×10^{21} cm^{-3}, i.e., a BM shift was not observed. For a rigid-band scheme of a heavily doped p-type semiconductor, E_F deepens with increasing n_{Hall} and the optical band gap should increase. The BM shift was estimated to be as large as 0.3 eV for $n_{Hall} = 1.7 \times 10^{21}$ cm^{-3} and $m_h^* = 1.6 m_e$. Hence, the simple rigid-band model is invalid for LaCuOSe:Mg.

The HX-PES spectra in Figure 3b demonstrated that heavy hole doping at $n_{Hall} = 1.7 \times 10^{21}$ cm^{-3} did not alter the VB

(36) Tampo, H.; Yamada, A.; Fons, P.; Shibata, H.; Matsubara, K.; Iwata, K.; Niki, S.; Nakahara, K.; Takasu, H. *Appl. Phys. Lett.* **2004**, *84*, 4412.
(37) Li, L.; Shan, C. X.; Wang, S. P.; Li, B. H.; Zhang, J. Y.; Yao, B.; Shen, D. Z.; Fan, X. W.; Lu, Y. M. *J. Phys. D: Appl. Phys.* **2009**, *42*, 195403.
(38) Katase, T.; Nomura, K.; Ohta, H.; Yanagi, H.; Kamiya, T.; Hirano, M.; Hosono, H. *Cryst. Growth Des.* **2010**, *10*, 1084.

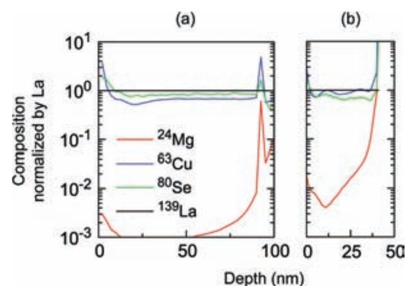

Figure 4. SIMS depth profiles of LaCuOSe epitaxial films: (a) nominally undoped film ($n_{Hall} = 2.5 \times 10^{19}$ cm^{-3}) and (b) LaCuOSe:Mg film (1.7×10^{21} cm^{-3}). Origin of the depth corresponds to the film surface, and the chemical compositions are normalized by that of La in the atomic ratio.

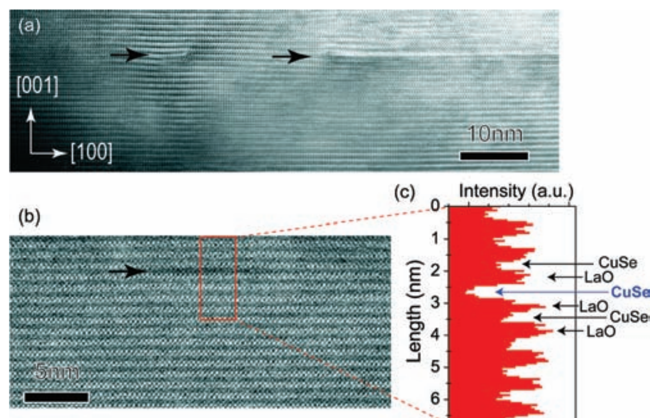

Figure 5. (a) HR-TEM image of LaCuOSe:Mg film ($n_{Hall} = 1.7 \times 10^{21}$ cm^{-3}). (b) Magnified STEM-HAADF image around a planar defect. Horizontal black arrows indicate planar defects. (c) Intensity profile taken from the square region in the STEM image.

structure and the position of E_F. This result was consistent with the absence of a BM shift. Therefore, we concluded that the holes are not doped in the VB of the stoichiometric LaCuOSe but that acceptor bands form just above the VBM.

III.3. Mg Doping and Hole Concentration. Next, we measured SIMS depth profiles to determine the chemical compositions of LaCuOSe films. Figure 4 shows the obtained atomic ratios normalized by that of La (the atomic ratios are expressed, e.g., by [La]). Although accurately determining the absolute compositions is difficult using SIMS, the nominally undoped sample ($n_{Hall} = 2.5 \times 10^{19}$ cm^{-3}, Figure 4a) exhibited a distinct trend. The Cu and Se concentrations were lower than those in the polycrystalline bulk LaCuOSe, which was used as the calibration reference, suggesting that the off-stoichiometry of Cu and Se is related closely to high-density hole doping even in a nominally undoped film. Such Cu and Se deficiencies were also observed for a heavily hole-doped LaCuOSe:Mg film ($n_{Hall} = 1.7 \times 10^{21}$ cm^{-3}, Figure 4b).

The [Mg]/[La] ratio in the LaCuOSe:Mg film was much lower ([Mg]/[La] $\approx$ 1%) than the chemical composition ([Mg]/[La] = 20%) of the PLD target. Assuming that mobile holes are generated by substitution of Mg^{2+} at the La^{3+} sites and all acceptor states are activated, [Mg] = 10% is required to explain the observed n_{Hall} value of 1.7×10^{21} cm^{-3}. However, the [Mg] value obtained by SIMS was smaller by an order of magnitude. Thus, the possibility that mobile holes are generated from the aliovalent substitution of Mg at the La sites could be excluded. The low Mg concentration in the epitaxial films may be a consequence of the postdeposition thermal crystallization employed in the R-SPE process, which eliminated Mg impurities in the films. This assertion is reasonable because the crystallization process in R-SPE is similar to that in the zone-refining method.[39] Hence, the Mg impurities diffused to the film surface and evaporated under a vacuum. The slight increase in the Mg concentration observed near the film substrate interface (Figure 4a and 4b) is thought to be due to the in-diffusion from the MgO substrates. Remembering the successful hole doping by Ca/Sr substitution at La sites in the bulk samples,[5] the Mg-doping effect is specific to the thin films. These observations indicate that the role of Mg doping is a kinetic one not a thermal equilibrium because most of the Mg ions were wiped out in the highly doped films.

III.4. Planar Defects Observed by Electron Microscopy. Figure 5 shows cross-sectional HR-TEM images of a heavily doped LaCuOSe:Mg epitaxial film ($n_{Hall} = 1.7 \times 10^{21}$ cm^{-3}), which clearly shows a layered contrast originating from the crystal structure composed of LaO and CuSe layers (Figure 5a) as well as two planar defects (indicated by the horizontal arrows). Figure 5b and 5c shows a STEM-HAADF image and the intensity profile of a selected area that includes the defect, respectively. The signal intensity in HAADF imaging is known to be roughly proportional to the square of the atomic number Z, which provides a high-contrast image for LaO, CuSe, and defect layers. Clear periodical signals corresponding to the LaO and CuSe layers (Figure 5 c) were observed, but the signals became very weak in the defect region corresponding to the CuSe monolayer. These observations indicated that the planar defect is composed of Cu and Se deficiencies, which is consistent with the SIMS result (Figure 4b). We note that such defects were also generated during the HR-TEM observations, suggesting that the actual density would not be as high as that observed in the present HR-TEM images. However, we can safely say that the planar defects due to Cu and Se deficiencies are easily created in LaCuOSe:Mg films and a very possible source of the hole doping.

IV. Discussion

IV.1. Doping of AE Ions (AE = Mg, Ca, Sr). To examine the above experimental results, we performed DFT calculations. First, AE doping (AE = Mg, Ca, and Sr) at the La sites was examined. Figure 6a shows E_{Form} for the AE substitutions in LaCuOSe. The E_{Form} values were estimated based on the chemical reactions of $(LaCuOSe)_{18}$ + AE (crystal) $\rightarrow$ $La_{17}AE_1Cu_{18}O_{18}Se_{18}$ + La (crystal). All the E_{Form} values were positive, indicating Mg doping is most unstable among these AE dopings. Here, we note that although we attempted aliovalent ion doping other than Mg, even Ca and Sr doping could not achieve the high-density hole concentrations above 1×10^{20} cm^{-3}.[18] Therefore, Mg doping is not likely the origin of the high-density hole doping, which is consistent with the low Mg concentration in the highly doped (1.7×10^{21} cm^{-3}) film observed by SIMS (Figure 4b).

IV.2. Point Defects. We then calculated E_{Form} of the point defects (Figure 6b). Similar chemical reactions to those above were assumed. For example, for the anion substitution models (Se_O and O_{Se} cases), $(LaCuOSe)_{18}$ + Se $\rightarrow$ $La_{18}Cu_{18}(O_{17}Se)Se_{18}$ + $1/2O_2$ and $(LaCuOSe)_{18}$ + $1/2O_2$ $\rightarrow$ $La_{18}Cu_{18}O_{18}(Se_{17}O)$ + Se were, respectively, employed. For V_{Cu}, $(LaCuOSe)_{18}$ $\rightarrow$

(39) Pfann, W. G. *Zone Melting*, 2nd ed.; John Wiley & Sons Ltd: New York, 1966; ISBN: 0471685100.

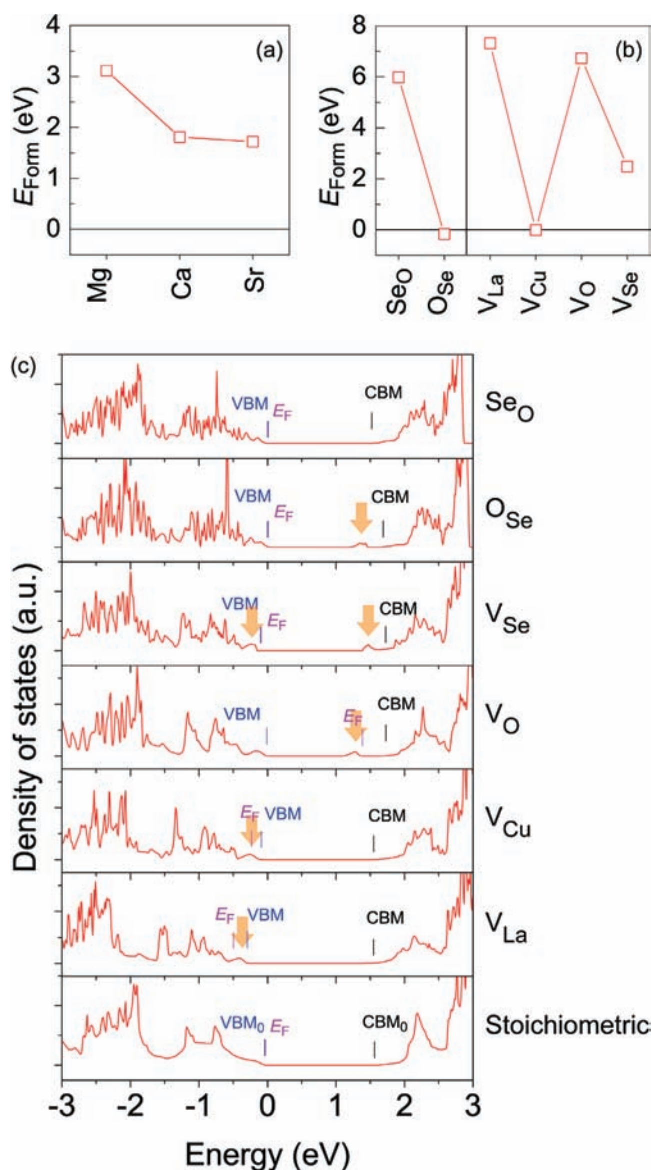

Figure 6. E_{Form} of the AE doping (AE = Mg, Ca, and Sr) at the La site (a) and point defects (b). (c) DOSs of the point-defect models. Arrows indicate the additional states upon introducing defects. Energy is aligned by La 5s at ca. −32 eV, and its origin corresponds to VBM_0.

$La_{18}Cu_{17}O_{18}Se_{18}$ + Cu (crystal) was employed, which is similar to those for other monovacancies. E_{Form} of the Se_O substitution defect was very large, ~6 eV, while that of O_{Se} was negative, indicating that Se ions are easily substituted by O ions if the synthesis/film growth atmosphere is oxygen rich, but substitution of a Se ion for an O ion would not occur even in an oxygen-poor atmosphere due to the large E_{Form} of Se_O. The large E_{Form} of Se_O is understood because the ion radius of Se^{2-} (198 pm) is much larger than that of O^{2-} (142 pm),[40] which requires large displacements of the coordinating Cu and La ions, while formation of the O_{Se} substitution only requires displacement of the O ion from the original Se site to a position closer to Cu. In addition, O−Cu and O−La bonds are stronger than Se−Cu and Se−La bonds, which also contribute to the large E_{Form} of Se_O and the negative E_{Form} of O_{Se}.

Among the monovacancies, only the E_{Form} of V_{Cu} was close to zero, whereas those for other vacancies were positive and larger than 2 eV, indicating that V_{Cu} is easily or even spontaneously created in LaCuOSe. As shown in Figure 6c, V_{La} and V_{Cu} can work as shallow acceptors because E_F is located below the VBM of stoichiometric LaCuOSe (hereafter denoted VBM_0). This result can be understood by considering the typical defect reaction of LaCuOSe → $M^0 + V_M^{n-} + nh^+$ (M = Cu and La). In particular, it has been proposed that V_{Cu} is the main origin of hole doping for other copper-based oxides, including Cu_2O and $CuAlO_2$.[41−44] For the anion vacancies, V_O shifts E_F closer to CBM but deep occupied states are formed (thick vertical arrow in Figure 6c. Note that DFT underestimates the bandgap values, and the absolute energy values from the CBM_0 of the in-gap states are not accurate.). However, V_{Se} does not change E_F, and the deep occupied states are formed below the VBM_0 (indicated by the left arrow). It is almost consensus that V_O forms in the deep occupied states in wide gap oxide semiconductors such as ZnO[45] and $InGaZnO_4$[46,47] where the electrons released from formation of an oxygen vacancy are trapped at V_O sites because V_O has rather large free spaces. This view explains why V_{Se} has a larger free space and forms the very deep trap states even below the VBM_0. Moreover, Se_O and O_{Se} do not shift E_F because their formal charges remain the same (−2), and these substitutions do not require extra charges to be generated. Considering that E_{Form} of V_{La} is very large and E_F of V_{Cu} and V_{La} are deeper than the VBM_0, we can conclude that V_{Cu} is the only possible origin for hole doping among these point defects. O_{Se}, V_{Se}, and V_O are candidates to explain the observed optical absorption because they form extra states below the conduction band minimum (CBM) of stoichiometric LaCuOSe (CBM_0).

IV.3. Complex Defects. Additionally, we examined complex defects. Figure 7 shows DOSs and E_{Form} of the clusters of V_{Cu}. As the number of $V_{Cu}(x)$ clusters increased, E_F shifted to a deeper energy and the hole concentration increased. Similar to the single V_{Cu} case, the subgap states did not form in all cases. Moreover, E_{Form} per vacancy (E_{Form}/x) increased as the number of V_{Cu} increased, but these values are less than 0.5 eV, indicating that monovacancies are most easily formed but other V_{Cu} complexes can also be created if x is small.

Figure 6b indicates that E_{Form} of V_{Cu} and V_{Se} are the smallest among the point defects. Additionally, we implied that V_{Cu} can explain p-type doping, whereas V_{Se} can explain the subgap absorption as observed in Figure 6c. The SIMS and STEM results for a heavily doped film indicate that the sample involves planar defects of V_{Cu} and V_{Se}. Hence, we considered complex defects around a Se ion, $V_{Cu} \times x + V_{Se}$ (x = 1−4) (Figure 8). In these complex vacancies, E_{Form} values were estimated using the following reaction: $(LaCuOSe)_{18} \rightarrow La_{18}Cu_{18-x}O_{18}Se_{17} + x$Cu (crystal) + Se (crystal). Among these defects, defects with x = 1, 3, and 4 worked as shallow acceptors because their E_F are located below VBM_0. Except for x = 4, these complex defects explain subgap absorption because these form subgap states, which are denoted by the right vertical arrows near the CBM

(40) Shannon, R. D. *Acta Crystallogr., Sect. A* **1976**, *32*, 751.

(41) Nolan, M.; Elliott, S. D. *Phys. Chem. Chem. Phys.* **2006**, *8*, 5350.
(42) Raebiger, H.; Lany, S.; Zunger, A. *Phys. Rev. B* **2007**, *76*, 045209.
(43) Nolan, M. *Thin Solid Films* **2008**, *516*, 8130.
(44) Tate, J.; Ju, H. L.; Moon, J. C.; Zakutayev, A.; Richard, A. P.; Russell, J.; McIntyre, D. H. *Phys. Rev. B* **2009**, *80*, 165206.
(45) Oba, F.; Nishitani, S. R.; Isotani, S.; Adachi, H.; Tanaka, I. *J. Appl. Phys.* **2001**, *90*, 824.
(46) Omura, H.; Kumomi, H.; Nomura, K.; Kamiya, T.; Hirano, M.; Hosono, H. *J. Appl. Phys.* **2009**, *105*, 093712.
(47) Kamiya, T.; Nomura, K.; Hirano, M.; Hosono, H. *Phys. Status Solidi C* **2008**, *5*, 3098.

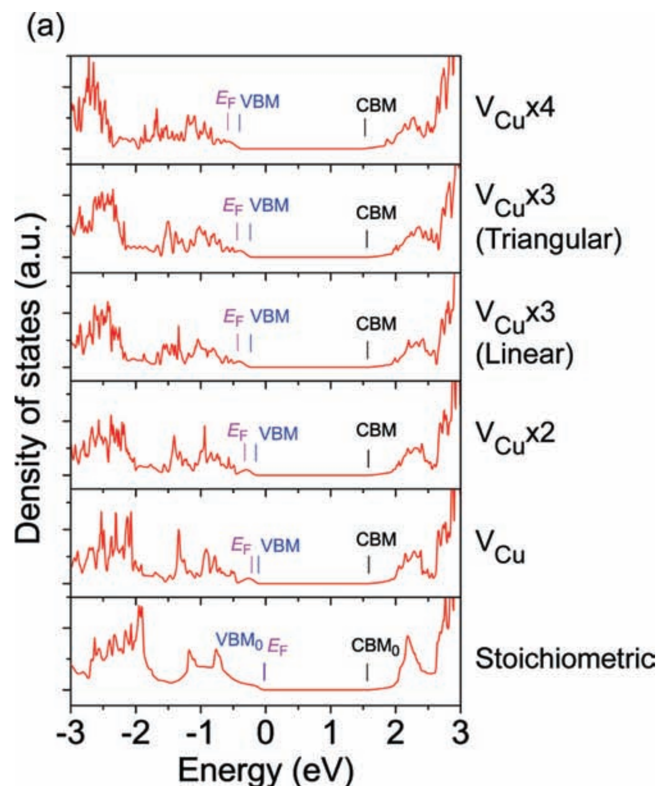

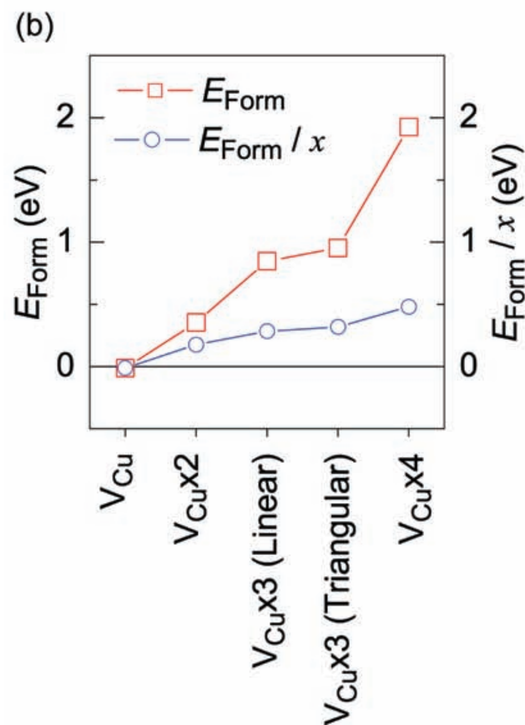

Figure 7. (a) DOSs of LaCuOSe: $V_{Cu} \times x$ ($x = 0-4$) models. For comparison, that of stoichiometric LaCuOSe is shown at the bottom. Energy is aligned by La 5s at ca. -32 eV, and its origin corresponds to VBM_0. (b) E_{Form} and E_{Form}/x (E_{Form} per V_{Cu}) of LaCuOSe: $V_{Cu} \times x$ ($x = 1-4$) models.

in Figure 8a. E_{Form} per vacancy ($E_{Form}/(x+1)$) was less than 0.5 eV for large complex defects of $x = 2-4$, indicating that these defects easily form in LaCuOSe. Although $V_{Cu} \times 2 + V_{Se}$ has a negative E_{Form} value, it cannot explain hole doping because it is a charge-neutral defect and E_F is located at the VBM.

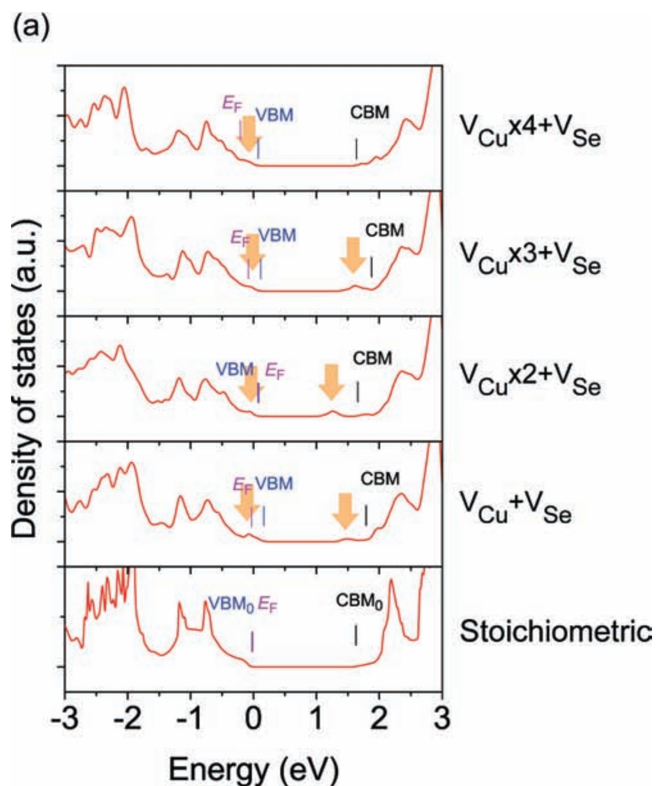

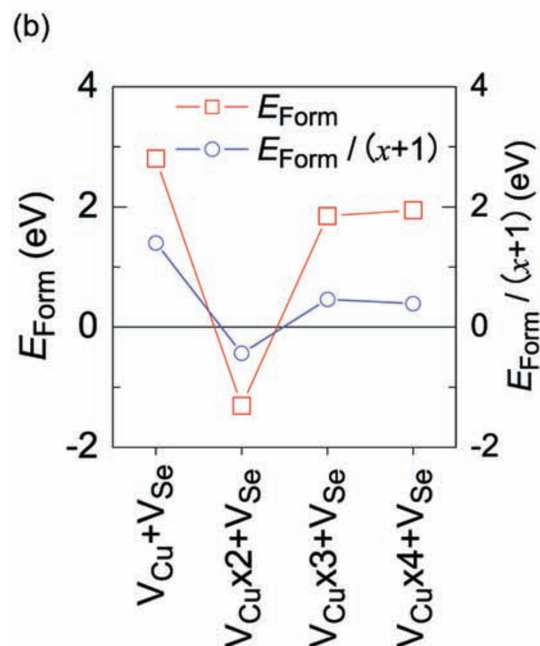

Figure 8. DOSs of LaCuOSe: $V_{Cu} \times x + V_{Se}$ ($x = 1-4$) models. For comparison, that of stoichiometric LaCuOSe is shown at the bottom. Energy is aligned by La 5s at ca. -32 eV, and its origin corresponds to VBM_0. (b) E_{Form} and $E_{Form}/(x + 1)$ (E_{Form} per vacancy) of LaCuOSe: $V_{Cu} \times x + V_{Se}$ ($x = 1-4$) models. Arrows denote the additional states upon introducing defects.

IV.4. Relation between Defect Models and Relevant Properties. Next, we analyzed the observation results of (I) the absences of a BM shift and E_F shift, (II) hole doping, (III) formation of the acceptor band above VBM (Figure 3b), and (IV) subgap optical absorption (Figure 3a). The schematic energy structure in Figure 9a shows that hole doping must result in the upper shift of the optical absorption edge, the disappearance of the exciton peaks, and the down shift of E_F if the band

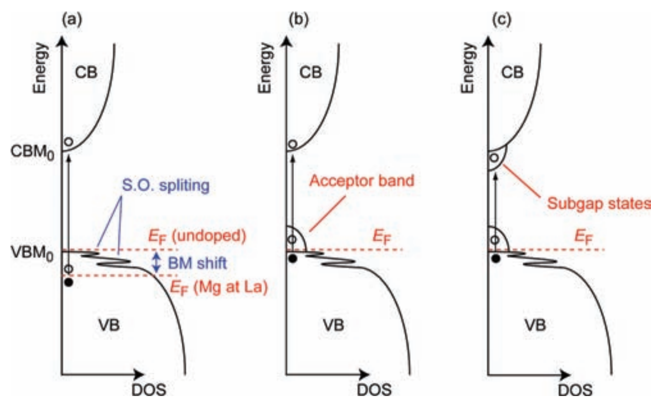

Figure 9. Electronic structure models for LaCuOSe:Mg: (a) simple rigid-band model, (b) acceptor band model, and (c) near-conduction band subgap state model. Table 1 summarizes the corresponding defect models. Closed and open symbols show the occupied and unoccupied states, respectively.

Table 1. Summary of DFT Results for Point- and Complex-Defect Models[a]

defect model	$E_{Form}/(x+1)$ (eV)	hole doping	acceptor band	subgap absorption
Se_O	+6.0	no	no	no
O_{Se}	−0.2	no	no	yes
V_{La}	+7.3	yes	no	no
V_{Cu}	−0.0	yes	no	no
V_O	+6.7	no	no	yes
V_{Se}	+2.5	no	no	yes
$V_{Cu} + V_{Se}$	+1.4	yes	yes	yes
$V_{Cu} \times 2 + V_{Se}$	−0.4	no	yes	yes
$V_{Cu} \times 3 + V_{Se}$	+0.5	yes	yes	yes
$V_{Cu} \times 4 + V_{Se}$	+0.4	yes	yes	no

[a] Columns of 'hole doping', 'acceptor band', and 'subgap absorption' indicate whether the calculated DOS of the corresponding model can explain the experimental results.

structure is rigid and the holes are doped into the VB of stoichiometric LaCuOSe. However, these expectations do not match the experimental results. The observations along with a high hole conductivity are consistently explained by the acceptor band model as illustrated in Figure 9b, but this model does not explain the subgap optical absorption because the acceptor bands are unoccupied states above E_F and the lowest energy optical transition should occur from VBM_0 to CBM_0. Therefore, additional unoccupied subgap states must exist below CBM_0 with an acceptor band above VBM_0 as illustrated in Figure 9c.

To reproduce the electronic structure illustrated in Figure 9c, the DOS of the appropriate defect model must satisfy the following features. (I) The VB of the defect model should have unoccupied states to explain the hole doping. (II) The VBM of the defect model should be higher than that of stoichiometric LaCuOSe to explain the acceptor band above VBM. (III) Subgap states should appear in the bandgap close to CBM_0 to explain the subgap optical absorption.

Table 1 summarizes these results as well as the calculated formation energies. It shows that hole doping is explained by V_{Cu}- or V_{La}-containing defects, including V_{Cu} clusters, but V_{La} is excluded because its E_{Form} is very large. O_{Se}, V_O, and V_{Se} can explain the subgap optical absorption, but V_O is excluded due to the large E_{Form}. The complex defects of $V_{Cu} + V_{Se}$ and $V_{Cu} \times 3 + V_{Se}$ can explain all the result, while the E_{Form} values are small but positive. Among all the defects examined, $V_{Cu} \times 2 + V_{Se}$ has the smallest $E_{Form}/(x + 1)$ of −0.4 eV and would be formed most easily in LaCuOSe; however, it does not explain hole doping because E_F is located at VBM. Considering these results, we conclude that multiple types of defects such as $V_{Cu} \times x + V_{Se}$ and V_{Cu} clusters coexist in LaCuOSe. Due to limitations of the model size, herein we considered small defects composed of several ions. As observed in the HR-TEM in Figure 5, the influence of extended planar defects composed of V_{Cu} and V_{Se} should also be important for a deeper understanding of carrier transport and doping in multicomponent semiconductors.

V. Conclusions

The hole transport properties and doping mechanisms in nominally undoped and Mg-doped LaCuOSe were examined to explain the observed electronic/optical properties, which appear contradictory within the framework of a simple rigid-band model (Figure 9a). The main origin of heavy hole doping up to 1.7×10^{21} cm^{-3} is the off-stoichiometry of Cu and Se and not Mg doping at the La sites. This conclusion is consistent with the chemical composition analysis and electron microscopic observations. However, our experience suggests that addition of Mg is necessary to obtain such high-density hole concentrations above 1×10^{20} cm^{-3}. Thus, we hypothesize that the added Mg ions enhance creation of Cu and Se deficiencies while these are diffused through the LaCuOSe layer during the thermal crystallization process of R-SPE. Ab initio calculations on defect-containing models also support the above conclusion and further indicate that complex Cu and Se defects explain the absence of a Burstein−Moss shift because an acceptor band is formed just above the valence band maximum (Figure 9b) whereas the subgap optical absorption is due to the subgap states formed below the conduction band minimum (Figure 9c).

Acknowledgment. The work at the Frontier Research Center was supported by the Japan Society for the Promotion of Science (JSPS), Japan, through the "Funding Program for World-Leading Innovative R&D on Science and Technology (FIRST) Program". The synchrotron radiation measurements were performed in beamline BL-47XU at SPring-8 with the approval of the Japan Synchrotron Radiation Research Institute (JASRI) (Proposal No. 2010A1638). The authors at The University of Tokyo were supported by a Grant-in-Aid for Scientific Research on Priority Areas "Nano Materials Science for Atomic Scale Modification 474" from the Ministry of Education, Culture, Sports, Science and Technology (MEXT) of Japan. This work was partially conducted in the Center for Nano Lithography and Analysis, The University of Tokyo, supported by the MEXT, Japan. The structure models in Figure 1 were drawn using VESTA.[48]

Supporting Information Available: Temperature dependences of carrier transport properties of LaCuOSe:Mg epitaxial films. This material is available free of charge via the Internet at http://pubs.acs.org.

JA107042R

(48) Momma, K.; Izumi, F. *J. Appl. Crystallogr.* **2008**, *41*, 653.